E-ISSN: 2706-8927
P-ISSN: 2706-8919
Impact Factor (RJIF):7.28
www.allstudyjournal.com
IJAAS 2025; 7(8): 134-141
Received: 28-08-2025
Accepted: 25-09-2025

Nam-Il Ri
Faculty of Mechanical Science and Technology, Kim Cheak University of Technology, Kyogudong No.60, Yonggwang Street, Pyongyang 950003, Democratic People's Republic of Korea

Kyong-Ryong Pae
Faculty of Mechanical Science and Technology, Kim Cheak University of Technology, Kyogudong No.60, Yonggwang Street, Pyongyang 950003, Democratic People's Republic of Korea

Kum-Song Ri
Faculty of Mechanical Science and Technology, Kim Cheak University of Technology, Kyogudong No.60, Yonggwang Street, Pyongyang 950003, Democratic People's Republic of Korea

Corresponding Author:
Kum-Song Ri
Faculty of Mechanical Science and Technology, Kim Cheak University of Technology, Kyogudong No.60, Yonggwang Street, Pyongyang 950003, Democratic People's Republic of Korea

Effects of axial clearance and liquid feed rate on the performance of liquid ring vacuum pump

Nam-Il Ri, Kyong-Ryong Pae and Kum-Song Ri

DOI: https://www.doi.org/10.33545/27068919.2025.v7.i10b.1715

Abstract
Numerical simulation of flow characteristics inside a liquid ring vacuum pump is carried out using the computational fluid dynamics (CFD) to investigate the effects of axial clearance and liquid feed rate on pump performance. The liquid ring vacuum pump with rotational speed of 2850 rpm was used for the numerical simulation. The axial clearance of the pump was changed to 0.1 mm, 0.2 mm and 0.3 mm, and the liquid feed rate was changed to 0.03 kg/s, 0.04 kg/s, and 0.05 kg/s. The results show that the impeller torque is the minimum when the axial clearance is 0.3 mm and the liquid feed rate is 0.03 kg/s, but the maximum compression pressure is 1.3 times smaller than that of the pump with 0.1 mm axial clearance and 0.05 kg/s liquid feed rate. The liquid injected through the liquid inlet flows toward the outlet region with increasing of the liquid feed rate and flows toward the inlet region with decreasing of liquid feed rate when the axial clearance is constant. And the liquid injected into the pump inside flows toward the inlet region with increasing of the axial clearance when the liquid feed rate is constant. The pressure distribution and the impeller torque of the pump are different with the change of axial clearances and liquid feed rates. The results of the research show that the axial clearance and the liquid feed rate of liquid ring vacuum pump have a significant influence on the pump performance.

Keywords: Liquid ring vacuum pump, gas-liquid two-phase, axial clearance, liquid feed rate, pump performance

Introductions
Liquid ring vacuum (LRV) pumps are widely used in the food, pharmaceutical, coal and chemical industries to create vacuum. LRV pumps are suitable for the exhaust of condensable, explosive, or corrosive gases because the exhaust process is isothermal compression [1, 2]. However, the efficiency of the LRV pump is generally low and power consumption is high [3-5]. Many works have been carried out by researchers to increase the efficiency and reduce power consumption of the pumps. Zhang *et al.* [6] experimentally verified that the maximum isothermal compression efficiency could be achieved by automatically adjusting the discharge area of the pump according to the suction pressure. Yu.V. Rodionov *et al.* [7] designed a pump body structure that the area of the vaneless space was reduced 36 %, which could reduce the friction of the liquid and save 35 % of the power consumption. V. I. Teteryukov [8] designed the optimized body profile for maximum suction capacity of the pump, which proved that this structure could increase the suction capacity by 45.7 % and the isothermal compression efficiency by 8.1 %. Researchers have analyzed the effect of working fluid on pump performance [9, 10]. Jinshi Li *et al.* [11] verified that low working temperature and high flow rate of liquid could reduce unnecessary power consumption by experiments on the temperature of working liquid. L. Ma *et al.* [12] claimed that the proper operation of the LRV pump could reduce the heat generation of the pump and the power consumption of the pump. U.S. Powle *et al.* [13] developed automatic control techniques for heat exchangers to ensure the cooling efficiency and stability of the pump because the working environment temperature affects the cooling of the pump. The radial clearance between the impeller and the pump casing has a great influence on the performance of the pump [14]. The pump is affected by manufacturing errors, installation errors, thermal expansion so that the axial clearance generally is selected within 0.2~1.0 mm. Renhui Zhang [15] analyzed the phase distribution of gas-liquid two-phase flow in the axial clearance by numerical simulation. The results showed that the gas-liquid two-phase distribution in the axial clearance affects the efficiency of the pump. However, the effect of working liquid feed rate was neglected. R.H. Zhang [16] considered the effect of radial clearance and blade profile on pump performance.

The researchers made an energy distribution model of the LRV pump with improved structure and improved efficiency by reducing the energy loss by reducing the friction force and the turbulent flow loss.
In this paper, we have performed numerical simulations of the LRV pump with axial clearance by ANSYS Fluent 19.2, which liquid injection into the pump body was considered. First, the gas-liquid two-phase distribution and the pressure distribution in the axial clearance according to the different liquid feed rates were discussed when the axial clearance was constant. Second, the gas-liquid two-phase distribution and the pressure distribution in the axial clearance according to the different axial clearances were discussed when the liquid feed rate was constant. Lastly, the variation of the pump impeller torque and compression ratio according to the different axial clearances and liquid feed rates were discussed.

2. Numerical simulation by CFD

2.1. Geometric model and computational domain

The model of the LRV pump used in the study is shown in Fig. 1.

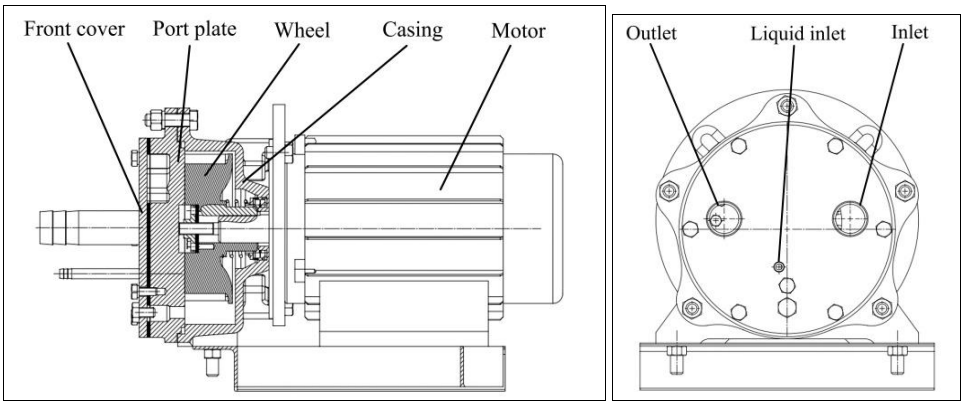

Fig 1: Structure diagram of test LRV pump. (a) Front view of test LRV pump. (b) Left view of test LRV pump.

The whole computational domain is divided into six regions: wheel, casing, liquid inlet, inlet, outlet, and axial clearance. The characteristics are shown in Table 1.

Table 1: The basic parameters of the modified LRV pump

Description	Value
Radius of pump casing (mm)	89
Axial width of impeller (mm)	50
Impeller diameter (mm)	154
Width of axial clearance (mm)	0.1, 0.2, 0.3
Radius of hub (mm)	35
Eccentricity (mm)	10
Number of impeller blades	14
Liquid feed rate (kg/s)	0.03, 0.04, .0.05
Rotational speed (r/min)	2 850
Wrap angle of impeller blade (°)	9.72
Inlet angle of impeller blade (°)	90
Outlet angle of impeller blade (°)	45
Thickness of the blade (mm)	4

In Fig. 1, the impeller rotates clockwise, and the working chambers in the crescent space are independent of each other by liquid ring and blades. When the impeller rotates, The gas sucked into the working chambers is compressed and exhausted through the outlet. The axial clearance is located between the impeller and the port plate. The computational domain is shown in Fig. 2.

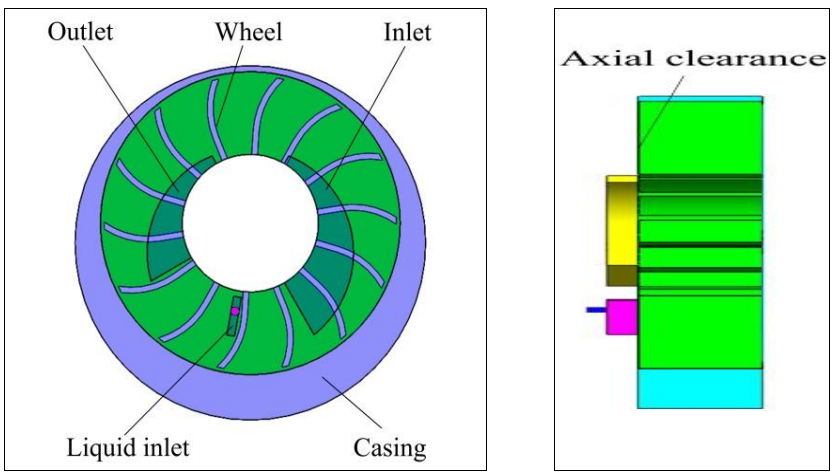

Fig 2: Computational domain of the LRV pump. (a) Front view of computational domain. (b) Left view of computational domain.

2.2. CFD model

2.2.1. Gas-liquid two-phase flow model

The fluid flow inside the LRV pump is gas-liquid two-phase flow. When the impeller rotates, the liquid forms a liquid ring with a shape similar to the pump casing under the action of centrifugal force, so that a crescent-shaped gas space and a free interface between the gas and the liquid ring are created in the inner space of the casing. VOF model is used to model multi-phase flow. The VOF model is more accurate in free-boundary processing than other multiphase flow models [17-20]. In the VOF model, the volume fraction variable α_v ($\alpha_v \in [0,1]$) is defined for each fluid in each computational cell. If α_v is equal to 1, the computational element is completely filled with specified fluid, and if α_v is equal to 0, it means that one fluid is empty and the another fluid is filled in the computational cell. If $0 < \alpha_v < 1$, It means that the free boundary of the two-phase flow exists in the computational cell. The transfer equation of the fluid volume fraction in a gas-liquid two-phase flow is given by equation (1).

$$\frac{\partial \alpha_v}{\partial t} + u_i \frac{\partial \alpha_v}{\partial x_i} = 0 \quad (1)$$

where t is the time; u_i is the velocity vector in the x_i direction; x_i is the coordinate variable.

2.2.2. Boundary conditions and turbulence flow model

The numerical simulation was simulated by ANSYS Fluent 19.2. Numerical simulations were performed for three-dimensional gas-liquid two-phase flow, which was unsteady. The rotor angular velocity was set to 2850 r/min, and the rotating and stationary domains were combined using a sliding mesh. To reduce the computational time, the gas phase was initialized in the inner region where the central coordinate was equal to the central coordinate of the casing and the diameter was smaller than 106 mm, and the water phase was set in the other region. The working fluid was set to water and the density of water was 998 kg/m^3. The surface tension coefficient was set to 0.07 N/m when the temperature was 20°C, and the gravitational acceleration was set to 9.81 m/s^2 in the negative direction of the Y-axis. The gas phase was set as ideal gas. The inlet boundary condition was set to constant mass flow rate and the fluid at the pump inlet was set to pure gas. The inlet mass flow rate of the gas was set to 0.02 kg/s. The outlet boundary condition of the pump was set to the static pressure 101325 Pa. The liquid feed rate was set at mass flow rate of 0.03 kg/s, 0.04 kg/s and 0.05 kg/s, respectively.

The turbulence model used the RNG k-ε model [21]. The RNG k-ε model is effective because it balances computational cost and computational accuracy compared to the LES model [22]. The pressure-velocity coupling was established by the PISO algorithm. A second-order central difference scheme was used to discretize the momentum equation. The residual error was set to 5×10^{-5}, and the flow field was considered convergent when the relative pulsation amplitude of the pump inlet pressure was less than 5 %. Considering the computational stability and upper limit of Courant number, the time step was set to 2×10^{-6} s. The time interval spent in performing the numerical calculations was 240 h. The simulation was run by a Dawning Parallel Server with 64 CPU cores.

3. Validation of model

3.1 Mesh generation and grid-independence test

A computational model with axial clearance was used to verify the validity of the model, which the axial clearance of model is equal to 0.2 mm. The computational domain was all divided into structured hexahedral meshes, which were implemented by ANISYS-ICEM software. The inlet liquid feed rate of the pump was set to 0.03 kg/s. The proper selection of the grids number and the improvement of the grid element quality are very important for numerical simulations of the computational domain. To determine the number of grids for the balance of computational cost and computational accuracy, models with five kinds of grids numbers were used for the calculations, whichgrids numbers were about 2.35 million, 3.63 million, 5.74 million, 7.54 million, and 9.42 million. The variations of inlet pressure according to the different grids numbers are shown in Fig. 3. Through the grid independence test, the computational cost and computational accuracy were balanced for the case with 7548362 grid cells. In this model, the axial clearance was divided into 15 layers. Near the solid wall, the grid cells were reconstructed. In this study, the first layer near the wall grid cell was set to 0.1mm, the increment ratio of the layer was set to 1.2, and the number of layers was set to 10. The mean y$^+$ value of the blade surface calculated by the RNG k-ε model is 3.2.

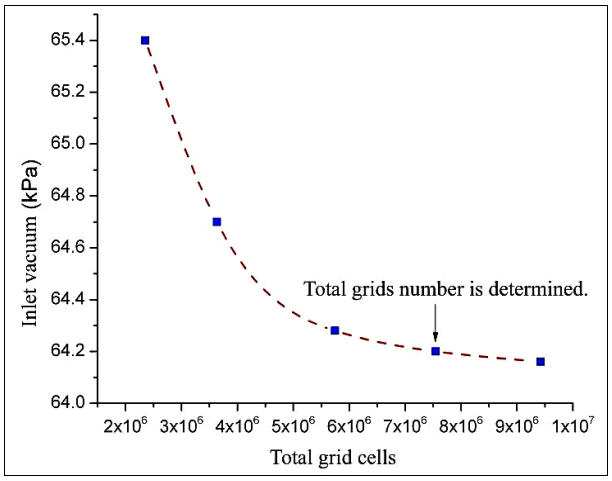

Fig 3: Grid independence test

3.2. Verification of CFD calculation accuracy

The experimental equipment of the LRV pump used in this paper is shown in Fig. 4.

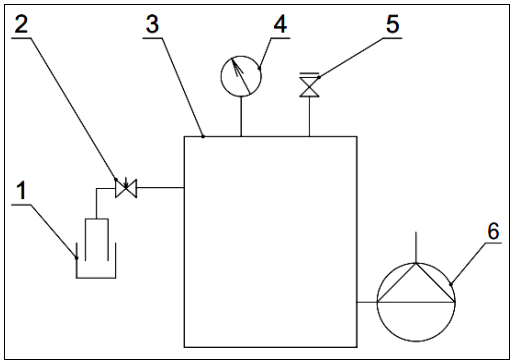

Fig 4: The experimental equipment of the LRV pump. 1-Gas flowmeter, 2-Needle valve, 3-Vacuum test vessel, 4-Vacuum gauge, 5-Vacuum breakdown valve, 6-LRV pump

The experimental equipment consisted of a LRV pump connected with an inlet pipe, an outlet pipe, flow meters, valves, a vacuum gauge and a vacuum vessel. The evacuation rate, inlet vacuum degree and shaft power cosumption of the pump were measured by a flowmeter, a pressure transducer and a dynamometer, respectively. Water was supplied to the pump at the rate of 0.03kg/s by a flowmeter connected to the liquid inlet. The measuring range of the flowmeter is 0 m^3/h to 1036 m^3/h and the measuring range of the vacuum gauge is -100 kPa to 0 kPa. The gas-liquid separator was installed in the outlet pipe to separate the gas and liquid that were discharged into the outlet of the pump. The hydrodynamic performance curves for the LRV pump were obtained and analyzed by numerical simulation and experimental measurements(Fig. 5).
The pump efficiency η can be calculated by equation (2).

$$\eta = \frac{p_1 Q_v \ln(p_2 / p_1)}{p} \quad (2)$$

Here p_1, p_2, p and Q_v are the inlet pressure, outlet pressure, shaft power and volume flow rate, respectively.

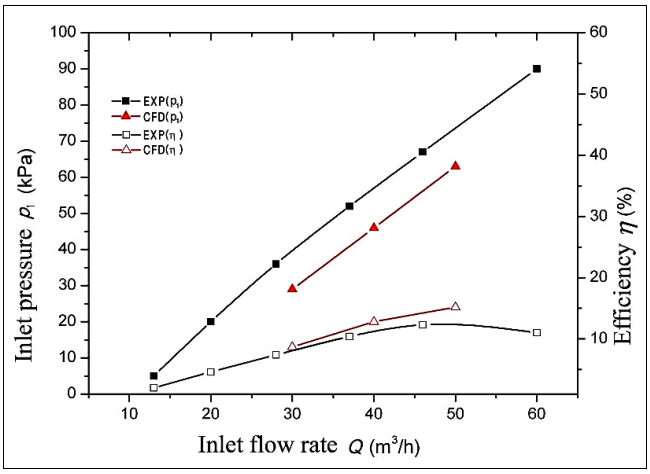

Fig 5: Comparison of experiments and simulations

In Fig. 5, the pump inlet pressure increases and the efficiency increases linearly with the increasing of flow rate. The figure also shows that the trend of the performance curves obtained by numerical simulation is almost similar to the experiment. The maximum error of the pump inlet vacuum is less than 5% difference from the experimental value. The main reason for the error between the simulation results and the experimental results is related to the grid quality and grids number of the model for the numerical simulation. Also, the reason is that the computational domain is not modeled exactly as the test pump. For example, the structure of chamfers, inlet and outlet was simplified for computational convenience. Lastly, the reason is that the effect of the liquid temperature injected is not taken into account. Since the simulation results and experimental results were similar when the evacuation rate of the pump was 40 m^3/h, this value was chosen to analyze the internal flow characteristics of the LRV pump in the next chapter.

4. Results and discussion

4.1. Analysis result of gas-liquid two-phase flow in the axial clearance of the LRV pump

There is no friction between the impeller and the port plate of the LRV pump, so there is inevitably a gap between them. This clearance forms a leakage path during operation and the gas leaks through the axial clearance from the compression region to the suction region. So the leakage of gas has a great effect on the ultimate pressure. The gas-liquid two-phase flow in the axial clearance of the LRV pump is considered to analyze the pump performance accurately. Fig. 6 shows the gas-liquid two-phase distribution in the axial mid-section of the LRV pump.

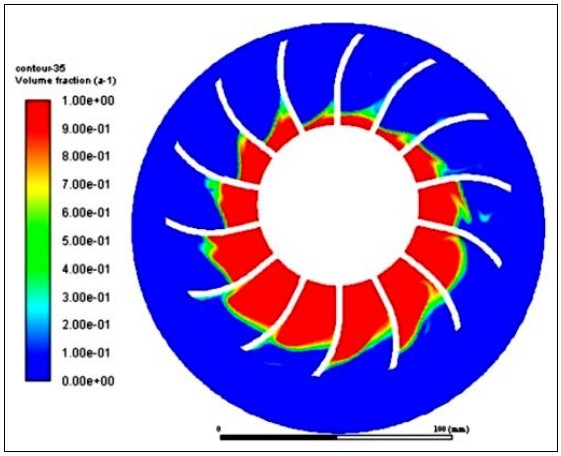

Fig 6: Gas-liquid two-phase distribution in the axial mid-section of the LRV pump

From Fig. 6, the formation of liquid ring inside the pump and the votex distribution of fluid at the tip of the blade are shown. The liquid forms a liquid ring similar to the structure of the casing under the action of centrifugal force by a high-speed rotating impeller during operation. Fig. 7 shows the pressure distribution in the axial mid-section of the LRV pump at t=0.025 s. From the figure, we can see that the inlet region of the pump is the low pressure region and the outlet region is the high pressure region. The gas sucked through the inlet is compressed by receiving energy from the liquid ring when the impeller rotates and is pumped through the outlet.

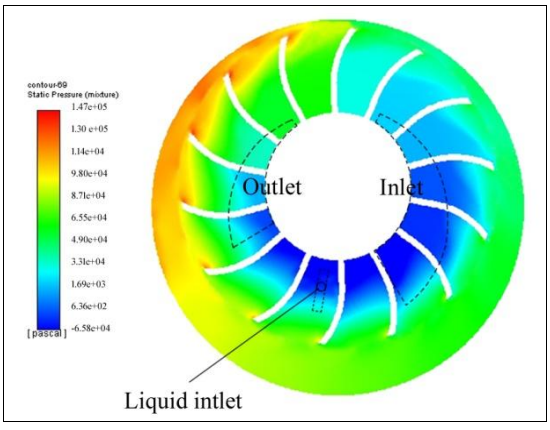

Fig 7: Pressure distribution in the axial mid-section of the LRV pump

Fig. 8 shows the gas-liquid two-phase distribution and pressure distribution in the axial clearance of LRV pump with an axial clearance of 0.1 mm and a liquid feed rate of 0.03 kg/s.

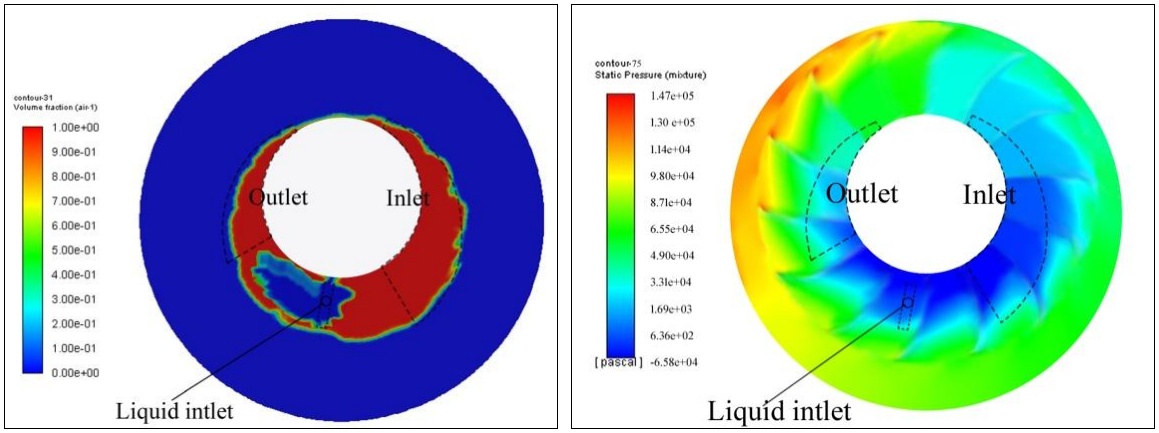

Fig 8: Gas-liquid two-phase distribution and pressure distribution in the axial clearance pump. (a) Gas-liquid two-phase distribution. (b) Pressure distribution.

Fig. 8 (a) shows the gas-liquid two-phase distribution in the axial clearance of the pump. In the LRV pump, the working chambers are formed by a liquid ring, blades, and a port plate, which adjacent cells are isolated from each other and suck, compress and discharge gase. In Fig. 8 (a), the adjacent cells are not completely sealed each other because there is an axial clearance between the impeller and the port plate. The LRV pump requires a continuous liquid supply to ensure cooling of the pump and seal between parts during operation. If the liquid injection is carried out through the axial clearance, the liquid film in the clearance can be formed to reduce the gas leakage between adjacent cells. Fig. 8 (b) shows the pressure distribution in the axial clearance of the LRV pump. The pressure of the axial clearance increases gradually from the suction region to the discharge region. Therefore, gas leaks from the high pressure cell to the low pressure cell. This is one of the main reasons why this pump cannot lower the ultimate pressure.

4.2. Analysis result of gas-liquid two-phase flow in axial clearance with variation of liquid feed rate and axial clearance

In the LRV pump, the liquid is supplied to the pump inside through the liquid inlet by the pressure difference between inside and outside of the pump. The liquid with a constant velocity passing through the liquid inlet is subjected to centrifugal force by the impeller, pressure force due to the pressure difference between the inlet and outlet regions, and viscous friction force in the axial clearanc between the impeller and the port plate. These forces depend on factors such as the liquid velocity through the liquid inlet, width of axial clearance, rotational speed of the impeller, liquid viscosity, pump suction pressure, etc. Fig. 9 shows the gas-liquid two-phase distribution and the liquid velocity vector in the axial clearance when the width of axial clearanc is 0.2 mm and the liquid feed rate is 0.03kg/s.

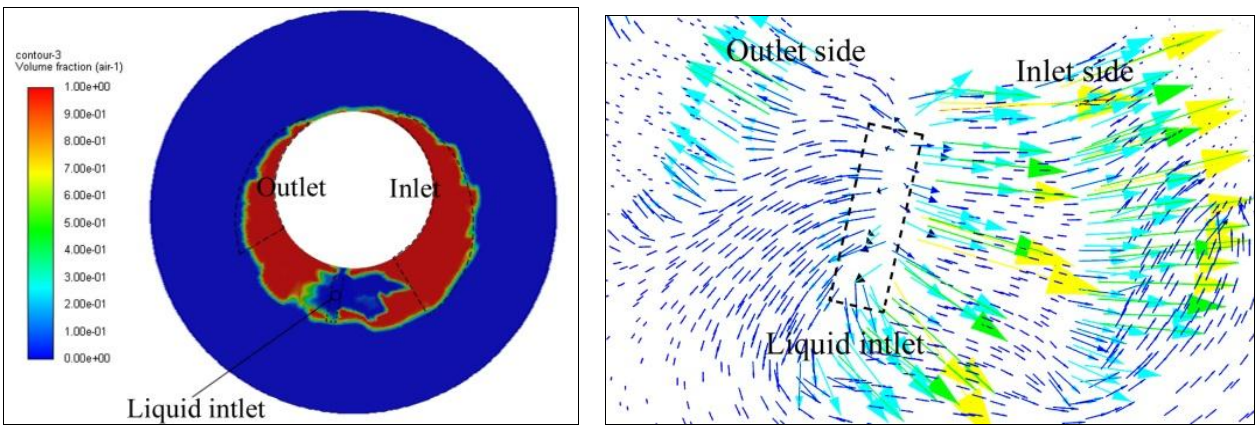

Fig 9: Gas-liquid two-phase distribution and velocity vector distribution of liquid in the axial clearance of LRV pump. (a) Two-phase distribution of gas-liquid in axial clearance. (b) Velocity vector of liquid in axial clearance

Fig. 9 (a) shows the gas-liquid two-phase distribution in the axial clearance. The liquid phase injected into the axial clearance is distributed much toward the inlet, which prevents the gas leakage through axial clearance between the liquid inlet and the inlet. Fig. 9 (b) shows the velocity vector distribution of the liquid in the axial clearance. When the axial clearance is 0.2 mm and the liquid feed rate is 0.03 kg/s, the liquid flows in the clearance toward the inlet region because the influence of pressure force by the pressure difference between the outlet and inlet regions is the stronger than the centrifugal force and the viscous friction force of the liquid by the impeller.

Fig. 10 shows the gas-liquid two-phase distribution and the liquid velocity vector in the axial clearance when the width of axial clearanc is 0.2 mm and the liquid feed rate is 0.05 kg/s.

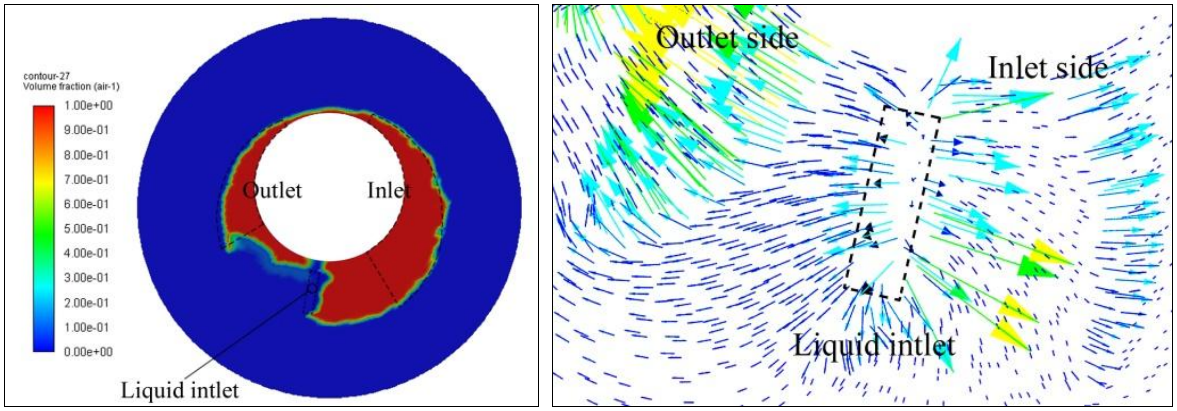

Fig 10: Gas-liquid two-phase distribution and velocity vector distribution of liquid in the axial clearance of LRV pump. (a) Two-phase distribution of gas-liquid in axial clearance. (b) Velocity vector of liquid in axial clearance

The liquid phase is distributed much in the axial clearance towards the compression region and the distribution of liquid phase in the inlet region is small (Fig. 10 (a)). Therefore, the distribution of liquid phase has a good effect on the sealing between the working cells of compression side. However, the sealing between the working cells of inlet side are not affected by it. Fig. 10 (b) shows the velocity vector distribution of the liquid phase in the axial clearance. The direction of the velocity vector of liquid phase is directed toward the outlet side because the centrifugal force and the viscous friction force of the liquid by the impeller are much larger than the pressure force between the outlet and inlet regions.

Fig. 11 and Fig. 12 show the pressure distribution in the axial mid-section of the pump with axial clearance of 0.2 mm when the liquid feed flow rates are 0.03 kg/s and 0.05 kg/s, respectively.

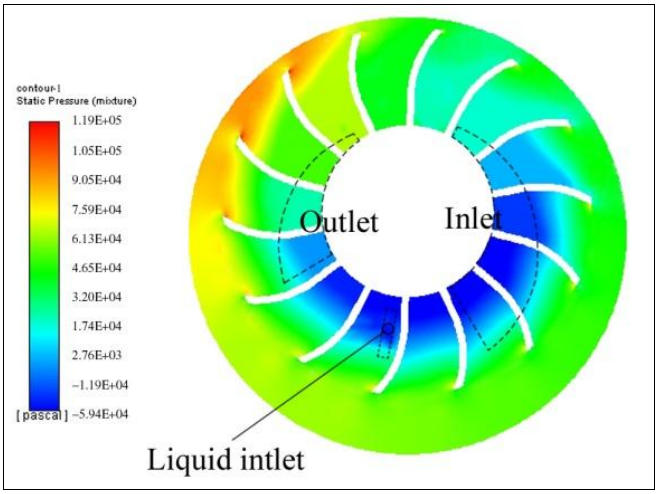

Fig 11: Pressure distribution in the axial mid-section of the pump with the liquid feed rate of 0.03 kg/s and the axial clearance of 0.2 mm

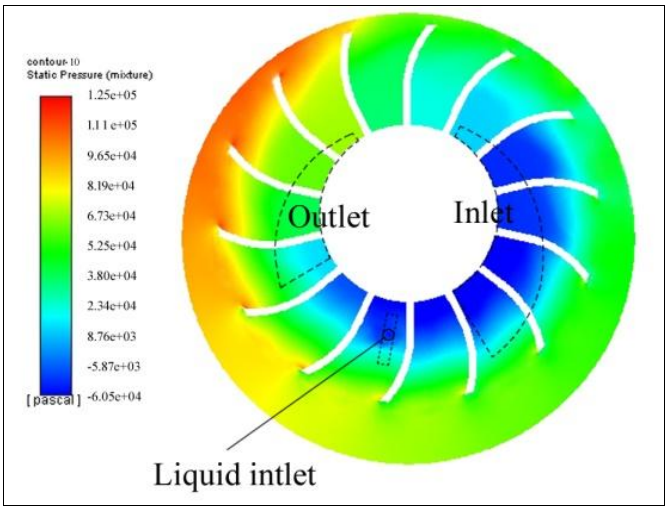

Fig 12: Pressure distribution in the axial mid-section of the pump with the liquid feed rate of 0.05 kg/s and the axial clearance of 0.2 mm

The figures show that the case of Fig. 12 presents a larger pressure in the compression region compared to the case of

Fig. 11. Increasing the liquid feed rate increases the compression ratio of the pump because the liquid film is well formed in the axial clearance.

4.3 Effects of axial clearance and liquid feed rate on the maximum pressure of the pump and the impeller torque

Increasing the liquid feed rate has a good effect on the liquid film formation in the axial clearance of the LRV pump, but the power consumption is also increased by it. So, the variations of the maximum compression pressures and the impeller torques were considered when the axial clearance of the pump was changed to 0.1 mm, 0.2 mm and 0.3 mm, and the liquid feed rate was changed to 0.03 kg/s, 0.04 kg/s and 0.05 kg/s, respectively. Fig. 13 shows the maximum compression pressure and the impeller torque when the axial clearance of the pump is changed to 0.1 mm, 0.2 mm and 0.3 mm.

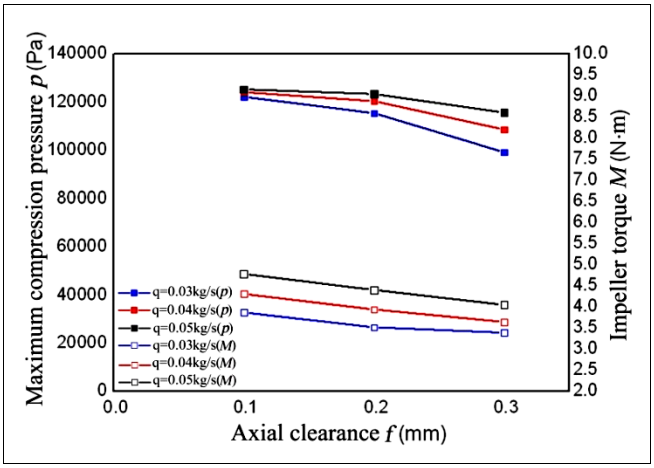

Fig. 13: Maximum compression pressure and the impeller torque when the axial clearance of the pump is changed to 0.1 mm, 0.2 mm and 0.3 mm

The maximum compression pressure and the impeller torque decrease with increasing clearance when the liquid feed rate of the pump is constant. Also, the maximum compression pressure and the impeller torque also increase as the liquid feed volume of the pump increases. Fig. 14 shows the maximum compression pressure and the impeller torque when the liquid feed rate of the pump is changed to 0.03 kg/s, 0.04 kg/s, and 0.05 kg/s, respectively.

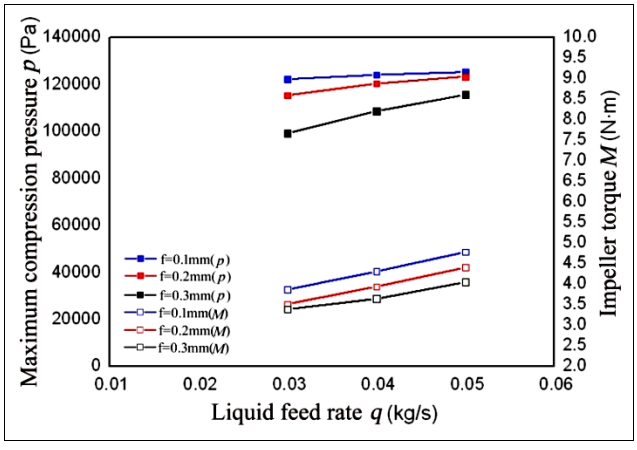

Fig 14: Maximum compression pressure and the impeller torque when the liquid feed rate of the liquid ring vacuum pump is changed to 0.03kg/s, 0.04kg/s, and 0.05kg/s

Both the maximum compression pressure and the impeller torque increase when the axial clearance of the pump is constant. The maximum compression pressure of the pump is 125382 Pa and the impeller torque is 4.7884 N•m when the axial clearance is 0.1 mm and the liquid feed rate is 0.05 kg/s. The maximum compression pressure of the pump is 95890 Pa and the impeller torque is 3.3944 N•m when the axial clearance is 0.3 mm and the liquid feed rate is 0.03 kg/s. As a result, the impeller torque of the pump with the axial clearance of 0.3 mm and liquid feed rate of 0.03 kg/s is the lowest. However, the maximum compression pressure in this case is 1.3 times less than the maximum compression pressure of the pump with the axial clearance of 0.1 mm and liquid feed rate of 0.05 kg/s.

5. Conclusion

In this paper, the numerical simulation of complex gas-liquid two-phase flow inside the LRV pump was investigated. From the simulation results, three conclusions can be drawn:

(1) The gas-liquid two-phase distributions in the axial clearance are different according to variation of the liquid feed rates when the axial clearance is constant. The liquid phase with the increasing of liquid feed rate is more distributed towards the outlet region compared to the inlet region. It is because the centrifugal and viscous friction forces of the liquid by the impeller are stronger than the pressure force by the pressure difference between the outlet and the inlet in the axial clearance.

(2) The gas-liquid two-phase distributions in the axial clearance are different according to the width variation of axial clearances when the liquid feed rate is constant, which has a great influence on the pump seal. When the axial clearance decreases, the liquid phase is more distributed toward the outlet region, and when the axial clearance increases, the liquid phase is more distributed in the inlet region.

(3) When the axial clearance and the liquid feed rate change, the impeller torque and maximum compression pressure of the pump change greatly. The smaller the axial clearance and the larger the liquid feed rate, the higher the maximum compression pressure and the impeller torque. The impeller torque is minimized when the axial clearanc is 0.3 mm and the liquid feed rate is 0.03 kg/s, but the maximum compression pressure is 1.3 times smaller than the case with axial clearance of 0.1 mm and liquid feed rate of 0.05 kg/s. When the axial clearance increases, the parts of the pump can be easily installed, but it is not possible to increase the compression ratio unless the liquid feed rate is increased. When the liquid feed rate increases, the compression ratio and impeller torque are increased. So the optimum clearance and liquid feed rate should be chosen to increase the compression ratio of the pump and reduce the impeller torque.

Acknowledgement

The work was carried out in Faculty of Mechanical Science and Technology of Kim Chaek University of Technology. The author would like to thank Mechanics Institute of the Faculty for their assistance in experimental part of the study. The author is thankful to the Head of the Department, Professor Hukjin.Song for his help and encouragement.

Conflict of interests
The author declares no conflict of interest.

Disclosure statement
No potential conflict of interest was reported by the authors.

Data Availability
The data that support the findings of this study are available within the article.

References

1. Powle US, Kar S. Investigations on pumping speed and compression work of liquid ring vacuum pumps. Vacuum. 1983;33(5):255-263.
2. Vertepoy YM, Matsenko VN, Antonov VM. Advances in water-ring vacuum pumps and compressors. Chem Petrol Eng. 1997;33(5):525-523.
3. Guo G, Zhang R, Jiang L, Yang J. Study on mechanism of unsteady gas-liquid two-phase flow in liquid-ring vacuum pump. Vacuum. 2024;222:242-250.
4. Wang J, *et al*. Geometric design and analysis of a novel sliding vane pump with three chambers. Mech Mach Theor. 2019;—.
5. Zhang RH, *et al*. Experimental study on gas-liquid transient flow in liquid-ring vacuum pump and its hydraulic excitation. Vacuum. 2020;—.
6. Zhang D, Liu Y, Kang J, Zhang Y, Meng F. The effect of discharge areas on the operational performance of a liquid-ring vacuum pump: numerical simulation and experimental verification. Vacuum. 2022;—.
7. Rodionov YV, Selivanov YT, Nikitin DV, Sychev MV, Kombarova PV. Novel construction of liquid ring vacuum pumps. Chemical & Petroleum Engineering. 2019;55(7-8):473-479.
8. Teteryukov VI. Effect of body shape on performance of water-ring vacuum pump. Chem Petrol Eng. 1966;2(8):511-513.
9. Chamoun M, Rulliere R, Haberschill P, *et al*. Modelica-based modeling and simulation of a twin screw compressor for heat pump applications. Appl Therm Eng. 2013;58(1-2):479-489.
10. Bianchi G, Cipollone R. Friction power modeling and measurements in sliding vane rotary compressors. Appl Therm Eng. 2015;84:276-285.
11. Li J, Zhou F, Zhang Y, Zhang D, Liu C, Kang J, Li N. Effect of working fluid temperature on energy dissipation characteristics of liquid ring vacuum pump. Appl Therm Eng. 2024;236:1-8.
12. Ma L, Cui F. Working principle and influence factors of water ring vacuum pump. Guangzhou Chem Ind. 2015;43(21):162-163+202. (In Chinese). DOI:10.3969/j.issn.1001-9677.2015.21.058.
13. Guo G, Zhang R, Yu H. Evaluation of different turbulence models on simulation of gas-liquid transient flow in a liquid-ring vacuum pump. Vacuum. 2020;180:109586.
14. Jang CM, Sato D, Fukano T. Experimental analysis on tip leakage and wake flow in an axial flow fan according to flow rates. J Fluids Eng. 2005;127(2):322-329.
15. Zhang R, Tian L, Guo G, Chen X. Gas-liquid two-phase flow in the axial clearance of liquid-ring pumps. J Mech Sci Technol. 2020;34(2):—.
16. Zhang RH, Yan LG, Yang JH. Influence of the radial gap and blade profile on the performance of the liquid-ring pump. Fluid Machinery. 2015;43(8):21-25. (In Chinese).
17. Li XW, Fan JF. A stencil-like volume of fluid (VOF) method for tracking free interface. Appl Math Mech. 2008;29(7):799-805.
18. Hirt CW, Nichols BD. Volume of fluid (VOF) method for the dynamics of free boundaries. J Comput Phys. 1981;39(1):201-225.
19. Zhang RH, Guo GQ, Yang JH. Investigation on inner gas-liquid flow and performance of liquid-ring pump. Trans Chinese Soc Agric Mach. 2014;45(12):99-103. (In Chinese).
20. Zhang RH, Wu H, Yang JH. Reconstruction for gas-liquid flow of the liquid-ring pump based on proper orthogonal decomposition. Trans Chinese Soc Agric Mach. 2017;48(6):381-386. (In Chinese).
21. Powle US, Kar S. Investigations on pumping speed and compression work of liquid ring vacuum pumps. Vacuum. 1983;33(5):255-263.
22. Guo G, Zhang R, Yu H. Evaluation of different turbulence models on simulation of gas-liquid transient flow in a liquid-ring vacuum pump. Vacuum. 2020;180:109586.